Dynamic Contrast-Enhanced and Diffusion MRI Show Rapid and Dramatic Changes in Tumor Microenvironment in Response to Inhibition of HIF-1α Using PX-478[1]

Bénédicte F. Jordan[*,†], *Matthew Runquist*[‡], *Natarajan Raghunand*[*], *Amanda Baker*[§], *Ryan Williams*[§], *Lynn Kirkpatrick*[¶], *Garth Powis*[§] *and Robert J. Gillies*[*]

*Department of Biochemistry, University of Arizona Health Sciences Center, Tucson, AZ 85724, USA; [†]Laboratory of Biomedical Magnetic Resonance, Université Catholique de Louvain, Brussels B-1200, Belgium; [‡]Department of Biotechnology, University of Arizona Health Sciences Center, Tucson, AZ 85724, USA; [§]Arizona Cancer Center, University of Arizona, Tucson, AZ 85724, USA; [¶]Prolx Pharmaceuticals, Tucson, AZ, USA

Abstract

PX-478 is a new agent known to inhibit the hypoxia-responsive transcription factor, HIF-1α, in experimental tumors. The current study was undertaken in preparation for clinical trials to determine which noninvasive imaging endpoint(s) is sensitive to this drug's actions. Dynamic contrast-enhanced (DCE) and diffusion-weighted (DW) magnetic resonance imaging (MRI) were used to monitor acute effects on tumor hemodynamics and cellularity, respectively. Mice bearing human xenografts were treated either with PX-478 or vehicle, and imaged over time. DW imaging was performed at three *b* values to generate apparent diffusion coefficient of water (ADCw) maps. For DCE-MRI, a macromolecular contrast reagent, BSA-Gd-DTPA, was used to determine vascular permeability and vascular volume fractions. PX-478 induced a dramatic reduction in tumor blood vessel permeability within 2 hours after treatment, which returned to baseline by 48 hours. The anti-VEGF antibody, Avastin, reduced both the permeability and vascular volume. PX-478 had no effect on the perfusion behavior of a drug-resistant tumor system, A-549. Tumor cellularity, estimated from ADCw, was significantly decreased 24 and 36 hours after treatment. This is the earliest significant response of ADC to therapy yet reported. Based on these preclinical findings, both of these imaging endpoints will be included in the clinical trial of PX-478.

Neoplasia (2005) **7,** 475–485

growth outstrips new blood vessel formation [2,3]. Hypoxic cancer cells survive the hostile hypoxic environment by changing to a glycolytic metabolism [4], becoming resistant to programmed cell death (apoptosis) [5] and producing factors such as vascular endothelial growth factor (VEGF) that stimulate new blood vessel formation from existing vasculature (angiogenesis), leading to increased tumor oxygenation and growth [6]. The cancer cell response to hypoxia is mediated through the hypoxia-inducible factor-1 (HIF-1) transcription factor [7,8]. HIF-1 is a heterodimer consisting of HIF1-α and HIF-1β subunits, both members of the basic−helix−loop−helix Per-ARNT-SIM (PAS) family of transcription factors [9]. HIF-1α and HIF-1β associate in the cytosol prior to transport to the nucleus [10] where they bind to hypoxic regulated element (HRE) DNA sequences in the 3′ and 5′ regions of hypoxia-regulated genes [11]. HIF-1β is constitutively expressed and its levels are not changed by hypoxia [7]. HIF-1α is constitutively expressed but, under aerobic conditions, it is rapidly degraded by the ubiquitin−26S proteasome pathway so that HIF-1α levels are almost nondetectable [12]. Under conditions of hypoxia, HIF-1α degradation is inhibited and HIF-1α protein levels increase, resulting in an increase in HIF-1 trans-activating activity.

HIF-1α expression has been detected in the majority of solid tumors examined including brain, bladder, breast, colon, ovarian, pancreatic, renal, and prostate tumors [13], whereas

Introduction

Solid tumors with areas of hypoxia are the most aggressive and difficult tumors to treat [1]. Even micrometastases have areas of hypoxia at the growing edge where tumor

no expression was detected in surrounding normal tissues, nor was it detected in benign tumors [14]. Clinically, HIF-1α overexpression has been shown to be a marker of highly aggressive diseases and has been associated with poor prognosis and treatment failure in a number of cancers including breast, ovarian, cervical, oligodendroglioma, esophageal, and oropharyngeal cancers [15–19]. HIF-1α presence correlates with tumor grade as well as vascularity [20,21]. High-grade glioblastoma multiforme has significantly higher levels of VEGF expression and neovascularisation compared with low-grade gliomas [22,23]. Studies such as these suggest that HIF-1 mediates hypoxia-induced VEGF expression in tumors, leading to highly aggressive tumor growth.

PX-478 (S-2-amino-3-[4′-N,N,-bis(2-chloroethyl)amino]-phenyl propionic acid N-oxide dihydrochloride) is a novel agent that suppresses both constitutive and hypoxia-induced levels of HIF-1α in cancer cells [24]. The inhibition of tumor growth by PX-478 is positively associated with HIF-1α levels in a variety of different human tumor xenografts in *scid* mice.

Magnetic resonance imaging (MRI) is a noninvasive technique that can be used to obtain information regarding tumor vascularization, metabolism, and pathophysiology, and allows early assessment of therapeutic effects of cancer drugs [25,26]. One approach is dynamic contrast-enhanced (DCE) MRI, which measures tumor vascular characteristics after administration of a contrast medium [27,28]. MRI enhanced with small-molecular-weight contrast agents is extensively used in the clinic to differentiate benign from malignant lesions, as well as to monitor tumor microvascular characteristics during treatment. However, the advantage of using large molecular agents (macromolecular contrast media, or MMCM) designed for prolonged intravascular retention has been demonstrated in several preclinical studies [29–32]. Correlations between MMCM-enhanced parameters and angiogenic markers such as microvessel density and VEGF levels have been studied [33,34]. Diffusion-weighted (DW) MRI allows noninvasive characterization of biologic tissues based on the random microscopic motion of water proton measurement, referred to as the apparent diffusion coefficient of water (ADCw) [35]. Preclinical studies have shown that DWI allows early detection of tumor response to chemotherapy [36–41]. Most likely, changes in the diffusion characteristics are caused by a shift of water to the extracellular space [42]. It is therefore anticipated that DW-MRI will detect early changes in cellular volume fractions resulting from apoptosis-associated cell shrinkage, necrosis, or vasogenic edema [43,44]. Because water is not as diffusionally restricted in the extracellular space, compared to the intracellular space, a decrease in cell volume fraction will result in an overall increase in the ADCw. We have previously characterized the capability of DWI to detect early changes in tumor ADCw following antitumor therapy in preclinical models [45,46] and in the clinical setting [47].

This study monitored the antitumor activity of PX-478, an HIF-1α inhibitor soon to enter clinical testing, on HT-29 human colon xenografts using both DCE and DW-MRI and assessed the use of these techniques as early and surrogate endpoints for the antitumor response to the drug. These noninvasive magnetic resonance techniques provide insights on tumor microvessel characteristics, such as PSP and vascular volume fraction, and on cellular volume ratios (cellularity and necrotic fraction), which may be early markers and even predictors of tumor response.

Materials and Methods

Cell Line and Tumor Implantation

HT-29, a tumorigenic nonmetastatic human colon carcinoma cell line, and A-549, a non small cell human lung cancer cell line, were obtained from the American Tissue Type Collection (Rockville, MD). Cells were passaged twice weekly with a 1:2 split and cultured in Dulbecco's modified Eagle's medium (DMEM:F12) supplemented with 10% fetal bovine serum (HyClone, Fort Collins, CO). For inoculation, approximately 10^6 cells in 0.1 ml of media were injected subcutaneously into the right flank of female severe combined immunodeficient (SCID) mice of ages 5 to 6 weeks (Arizona Cancer Center Experimental Mouse Shared Services, Tucson, AZ). Mice developed palpable tumors within a week of inoculation. Tumors were allowed to grow to 100 to 500 mm^3 prior to imaging. All animal protocols were approved by the University of Arizona Institutional Animal Care and Use Committee (IACUC; Tuczon, AZ).

Treatments

PX-478 was provided by Prolx Pharmaceuticals (Tucson, AZ) and prepared fresh each day in 0.9% NaCl as a 10 mg/ml solution and administered intraperitoneally to the mice within 30 minutes of preparation. Mice were treated with either vehicle or 125 mg/kg PX-478, and were studied 2, 12, 24, or 48 hours later. A minimum of eight animals were examined with MRI at each time point (four to six controls, and four to six treated). An additional 36-hour time point was included in the DW-MRI protocol. For imaging, mice were anesthetized using 1.0% to 2.0% isoflurane carried in oxygen. Body temperature was maintained at 37°C with a circulating water blanket and was monitored using a rectal Luxtron fluoroptic thermometer (Luxtron, Santa Clara, CA). Contrast agent, Gd-DTPA, coupled to albumin (Gd-BSA, 0.6 mg/g in 0.15 ml of saline), was injected by a tail vein catheter comprising a 30-gauge needle connected to PE-20 polyethylene tubing. The Gd-BSA was synthesized by the Arizona Cancer Center Synthetic Chemistry Core (Tucson, AZ). Chemical analysis indicated that there were an average of 3.8 Gd bound per protein molecule. The human anti-VEGF antibody Avastin (bevacizumab; Genentech, San Francisco, CA) was administered intravenously at a dose of 20 μl/30 g.

MRI

All imagings were performed on a 4.7-T horizontal bore MR imager (Bruker, Billerica, MA). Mice were positioned into a 24-mm ID Litzcage coil (Doty Scientific, Columbia, SC). Sagittal scout images were obtained to determine the position of tumors.

DW-MRI methodology.   Contiguous axial 2.0-mm slices covering the entire tumor were imaged as per the following protocol. DW images were obtained using the DIFRAD sequence [48], with the acquisition parameters: TR = 2 seconds, TE = 36 milliseconds, Δ = 13 milliseconds, δ = 5 milliseconds, matrix size = 128 × 128, and FOV = 4 × 4 cm, where δ and Δ represent the duration and separation of diffusion gradients, respectively. At each slice location, images were obtained at three *b* values (25, 500, and 950 sec/mm^2), with a time resolution of 13 minutes for a complete data set. The *b* value is equal to $\gamma^2 G_d^2 \delta^2 (\Delta - (\delta/3))$, where G_d is the strength of the diffusion weighting gradient and γ is the gyromagnetic ratio for protons. Images were reconstructed using a filtered backprojection algorithm of magnitude data to minimize motion artifacts. ADCw maps were generated by fitting the three *b* values to the Stejskal-Tanner equation, $S = S_0 e^{-b\text{ADCw}}$, where S_0 is the signal intensity in the absence of diffusion weighting and S is the signal intensity with diffusion weighting. ADCw maps were analyzed using programs written in Interactive Data Language (Research Systems, Boulder, CO). Hand-drawn regions of interest (ROIs) corresponding to tumor localized on the scout scans were cloned onto the ADCw maps, and ADCw distribution histograms were obtained for each tumor. For each time point (2, 12, 24, 36, and 48 hours after vehicle or PX-478 injection), two groups (one control and one treated) of four to six mice were imaged. In addition, four mice were monitored over the full time course, independently of the DCE-MRI protocol, to confirm the pattern observed on separate groups of mice.

DCE-MRI acquisition and analysis.   Contiguous axial 2.0-mm slices covering the entire tumor as well as a slice over the kidneys were imaged in the following protocol. A proton density–weighted (TR = 8 seconds, TE = 5.9 milliseconds, NA = 2, and FOV = 4 × 4 cm) and a T_1-weighted spin-echo image (TR = 300 milliseconds, TE = 5.9 milliseconds, NA = 8, and FOV = 4 × 4 cm) were collected prior to injection of contrast. A dynamic series of spin-echo images (TR = 300 milliseconds, TE = 5.9 milliseconds, NA = 4, FOV = 4 × 4 cm, and NR = 19) were collected over 45 minutes, with the contrast agent solution being injected during repetitions 2 to 5.

Signal enhancement in the DCE data was converted to albumin–Gd-DTPA concentration using the relaxivity of 1.08 l/g s measured *in vitro* at 37°C. This can be converted to 64.8 mM albumin/sec, assuming a M_W of 60 kDa. Enhancement was converted to concentration by assuming a linear relationship between Gd concentration and relaxation rate enhancement. These [albumin–Gd-DTPA] *versus* time data were fitted to a straight line for each pixel to obtain a *slope* (related to vascular permeability times the vascular surface area, PSP) and *y-axis intercept* (related to the vascular volume). In the absence of vascular volume changes, the PSP is referred to as simply as "permeability."

The vascular volume (VV) parameter measured in tumor pixels was normalized to the mean value obtained in an ROI placed on a muscle in the same animal and multiplied by 5% (~ VV fraction of the muscle) to convert it to the vascular volume fraction of the tumor. To be able to compare values between different mice, the slope parameter was normalized for Gd dose as follows for each mouse. The mean slope parameter calculated from pixels falling within the vena cava was used to normalize the slope determined in the tumor. The vena cava was identified using a hand-drawn ROI of approximately 5 to 10 pixels. Data analysis was performed using programs written in Interactive Data Language (Research Systems).

Antitumor Studies

The doses of PX-478 used for antitumor studies were 80 mg/kg daily for 5 days for the HT-29 colon cancer xenograft mice and 100 mg/kg daily for 5 days for the A-549 lung cancer xenograft mice. There were eight mice in each group. Tumor volume was measured twice weekly until the tumor reached 2000 mm^3, or became necrotic, at which point the animals were euthanized. Orthogonal tumor diameters (d_{short} and d_{long}) were measured twice weekly with electronic calipers and converted to volume by the formula: volume = $(d_{short})^2 (d_{long})/2$. Log$_{10}$ cell kill was calculated by the formula: log$_{10}$ cell kill = (tumor growth delay [day]) / (tumor doubling time [day] × 3.32). One-way analysis of variance using the general linear model was used to test for the effect of treatment on tumor growth rate and growth delay.

HIF-1α Immunohistochemistry

Paraffin-embedded tumor sections were heated at 60°C for 30 minutes and rehydrated through xylene and graded alcohols. Antigen retrieval was at 40 minutes at pH 9.0 for HIF-1α. The slides were blocked for 30 minutes in 4% milk, 1% goat serum, and 0.1% thimerosal in phosphate-buffered saline (PBS). After blocking, the slides were processed using a Ventana Medical Systems ES autoslide stainer. Endogenous peroxidase activity was quenched using a hydrogen peroxide–based inhibitor (DAB Basic Detection Kit; Ventana Medical Systems, Tucson, AZ) and endogenous biotin blocked using an AB Blocking Kit (Ventana Medical Systems). The slides were incubated for 32 minutes at 42°C with the mouse monoclonal antihuman HIF-1α (Transduction Laboratories, Lexington, KY) at 10 g/ml. A biotinylated universal secondary antibody, which recognized mouse IgG/IgM, was applied, followed by horseradish peroxidase–conjugated avidin, DAB/ hydrogen peroxide, and a copper enhancer. The slides were dehydrated through graded alcohols, toluene and xylene, and coverslipped using Vectamount (Vector Laboratories, Burlingame, CA). HIF-1α staining was normalized to the staining of an onslide control of hypoxic HT-29 colon cancer cells.

VEGF Detection

Plasma was collected into EDTA tubes and tumors were removed and immediately snap-frozen in liquid nitrogen. Tumors were then placed in buffer (10 mM Tris/HCl, pH 7.4, and 100 mM NaCl) and homogenized using a PowerGen 125 (Fisher Scientific, Pittsburg, PA). The

suspension was then centrifuged twice at 8000g at 4°C for 15 minutes. Protein was quantitated in a supernatant using the Pierce (Rockford, IL) BCA assay. VEGF levels were quantitated in plasma and tumor lysates using both human (hVEGF) and mouse VEGF (mVEGF) ELISA (R&D Systems, Minneapolis, MN), according to the manufacturer's instructions.

Statistical Analysis

Data are presented as the mean and standard error of the mean (SEM). Two-tailed Student's t tests, ANOVA, or Mann−Whitney rank sum tests were used where appropriate. $P < .05$ was considered to be statistically significant.

Results

### Effect of PX-478 on HT-29 Tumor ADCw

DW-MRI was used to detect the early response of HT-29 tumor xenografts to the antitumor agent, PX-478. A single gradient direction was used in this study because previous studies have shown the absence of anisotropy in extracranial tumor models [46,49]. ADC maps from representative animals at different times posttherapy are shown in Figure 1. Changes in mean tumor ADCw values over time, posttreatment, are presented in Figure 2. No change in ADC distribution was observed in sham-treated animals (Figure 2). At early time points (2 and 12 hours), ADCw values were not significantly different between control and treated groups. A substantial increase in mean relative tumor ADCw was observed for the treated groups at 24 and 36 hours posttreatment (94.5 ± 4.8%, $P = .005$, and 38.4 ± 4.9%, $P = .01$, respectively) before returning to pretreatment mean ADCw values by 48 hours posttreatment (nonsignificant change of 2.5% ± 6.7%, $P = .38$). ROIs defining the tumor were used to generate histograms of tumor ADCw values. ADCw histograms of individual tumors were then summed for each time point (Figure 2). A right shift in tumor water diffusion beginning by 24 hours after therapy is shown in Figure 2. Water diffusibility was still increased by 36 hours posttreatment and appeared to return to pretreatment values by the second day after therapy. This significant change in ADC (by 24 hours) occurs sooner than in other reports.

Effects of PX-478 on HT-29 Tumor DCE-MRI Parameters

Extravasation of the Gd-BSA was assumed to be describable by a PSP-limited two-compartment model with unidirectional transport of contrast agent on the timescale of our DCE-MRI experiments.

Parameter maps of "permeability" and vascular volume fraction were created to visualize the heterogeneity of tumor hemodynamic parameters. Heterogeneities in the distributions of pharmacokinetic parameters have previously been shown in experimental as well as in human tumors. Typical permeability (P) and vascular volume fraction (VV) maps at each time point are shown in Figure 3. Tumors were identified on proton density−weighted images and delineated by hand-drawn ROIs. Tumor vascular PSP is dramatically decreased in the PX-478 group 2, 12, and 24 hours after treatment in comparison with the control group (Figure 3A).
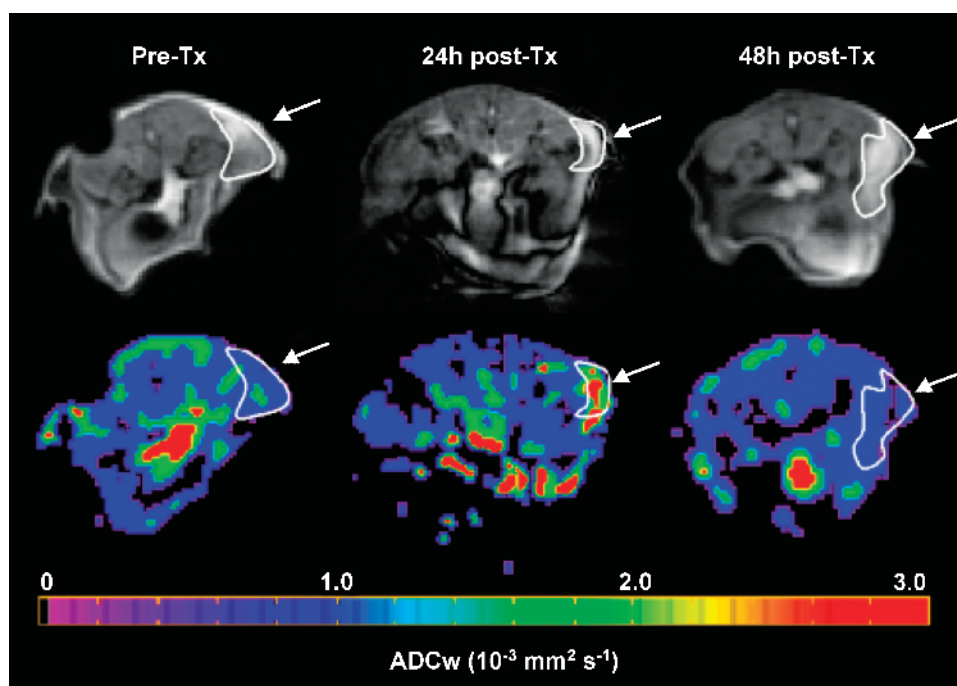
Figure 1. *DW images at a b value of 25 (up) and corresponding diffusion maps (bottom) of an HT-29 tumor-bearing mouse before, 24 hours, and 48 hours after PX-478 injection. Each image represents an axial slice of the mouse with the tumor area encircled and indicated by an arrow.*
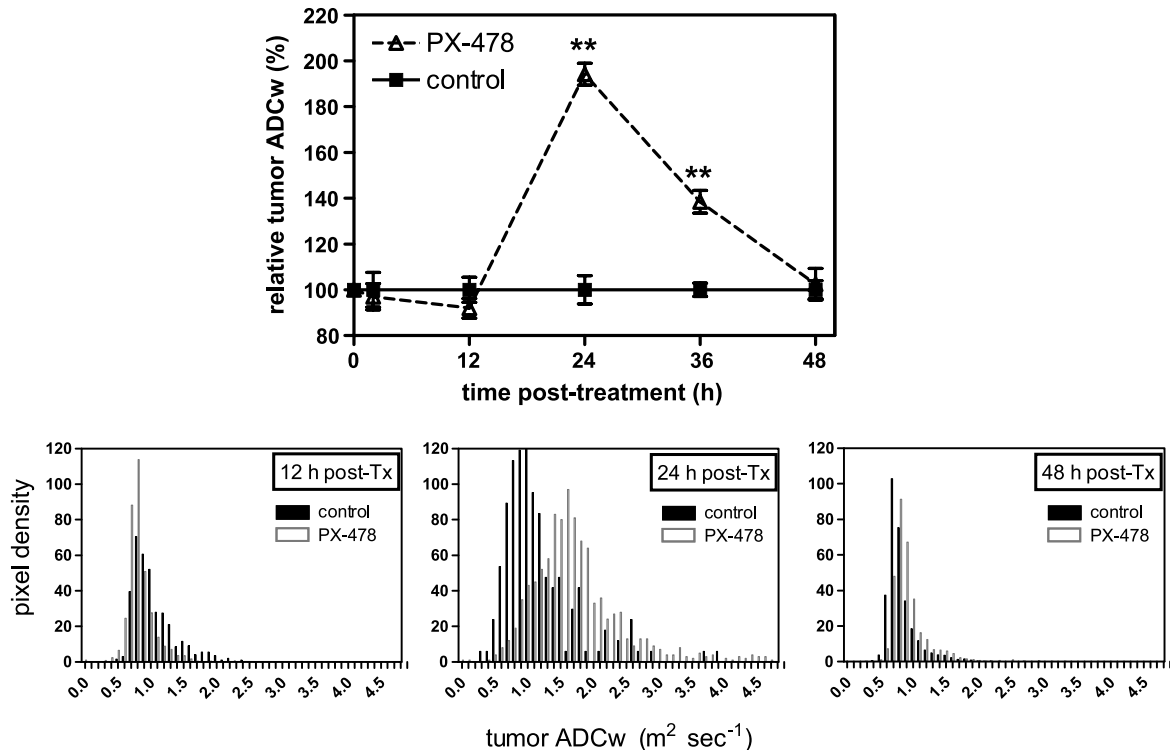
Figure 2. *Top: Full time course of average tumor ADCw following PX-478 administration (control mice, full line; treated mice, dotted line). A significant increase in average tumor ADCw is observed at 24 and 36 hours posttreatment. Bottom: Summed ADCw histograms of control (filled bars) and treated tumors (open bars) at each time point. A right shift in tumor ADCw is observed at 24 and 48 hours posttreatment.*

This decrease is no longer observed by 48 hours after treatment. Although some individual changes (positive or negative) in tumor vascular volume fraction were sometimes observed (Figure 3B; 2 and 24 hours posttreatment), the mean change between groups was not statistically significant. Hence, we conclude that the mechanism underlying the change in PSP is due to alterations in permeability, with little or no change in surface area, because surface area changes will also be reflected in the vascular volume estimation.

Time courses of mean normalized values and mean VV fraction values are presented in Figure 4 (relative data) and Table 1 (normalized values). A rapid decrease in tumor blood vessel permeability was observed within 2 hours after drug administration compared to control tumors, with a mean reduction of 73.3 ± 13.9% ($P = .012$). The decrease in permeability was still 72.4 ± 6.9% at 12 hours after treatment ($P = .003$). The effect progressively decreased in later time points, with a mean reduction of 55.0 ± 10.3% ($P = .02$) at 24 hours posttreatment and a return to control values at 48 hours (3.9 ± 10.9 %, $P = .71$, not significant). By contrast, the vascular volume fraction of the tumor was not significantly modified at any time point and remained unchanged between control and treated tumors.

Histogram analyses of these data lose spatial information yet retain the distribution of values for quantitative analyses. Figure 5 shows histogram data summed for all animals in each group. Control tumors at each time point (filled bars in each plot) were characterized by heterogeneous and broad distributions of ''permeability'' values at all time points. In contrast, treated tumors showed more homogeneous and narrow histograms centered around much lower values at 2, 12, and 24 hours (open bars). Note that the range of median of the distribution of permeability values returned to control levels at 48 hours. These data can also be further reduced to median values (dashed vertical lines in each population), which were significantly decreased in the treated groups 2, 12, and 24 hours after treatment.

Effects of Anti-VEGF Antibodies on HT-29 Tumor DCE Parameters

To assess the ability of the MMCM DCE technique to detect acute changes after treatment with an antitumor agent aimed at decreasing VEGF in this tumor model, human anti-VEGF antibody (Avastin) was administered to HT-29 tumor-bearing mice. A 75.0 ± 4.0 % decrease in vascular PSP was observed within an hour of injection of the antibody ($P < .0001$), similar to the changes observed 2 and 12 hours after PX-478 administration (Figure 6A, Table 1). The anti-VEGF antibody treatment also induced a significant 31.5 ± 2.6 % ($P = .023$) decrease in vascular volume fraction, unlike treatment with PX-478 (Figure 6A, Table 1). Hence, in this case, the PSP changes may not be entirely due to permeability, and may also involve alterations in the vascular surface area.

Effects of PX-478 on A-549 Tumor DCE Parameters

A-549 non small cell lung tumors are resistant to PX-478 (Antitumor Studies section and Ref. [24]) and were therefore used as negative controls for the DCE-MRI protocol. No significant change was observed for either tumor permeability or vascular volume fraction (Figure 6B, Table 1). These data suggest that the changes observed on HT-29 xenografts after administration of PX-478 are connected to the sensitivity of this tumor model to the drug. Notably, the untreated PSP values of A-549 tumors were lower than the control values obtained in HT-29 tumors, suggesting that baseline PSP values may be prognostic for the antitumor effects of PX-478, although further investigation is required.

### Antitumor Effect of PX-478 on HT-29 and A-549 Xenografts, HIF-1α Staining, and VEGF Detection

HT-29 colon cancer xenografts exhibited staining for HIF-1α, whereas A-549 non small cell lung cancer xenografts showed very little staining (Figure 7). The A-549 lung cancer xenografts showed no growth inhibition when treated with PX-478 (100 mg/kg, i.p.) daily for 5 days, whereas the HT-29 colon cancer xenografts exhibited a tumor growth delay of 16 days with a calculated log cell kill of 1.6 ($P < .05$). The lack of responsiveness to PX-478 by A-549 tumors is probably due to the lack of HIF-1α expression in these tumors compared to HT-29 xenografts (Figure 7). The lower permeability observed is probably explained by the lower expression of VEGF-A, an HIF-1 target gene. Levels of

VEGF-A are also markedly lowered in A-549 tumors *versus* HT-29 tumors (50.12 ± 12.09 *vs* 1.81 ± 0.23 pg/μg, $P = .012$, Mann−Whitney rank sum test) as measured by ELISA.

Discussion

The activity of PX-478, an inhibitor of HIF-1α in experimental tumors, was evaluated on HT-29 human colon xenografts using both DCE and DW-MRI. PX-478 induced a substantial reduction in tumor blood vessel permeability as early as 2 hours after a single dose of 125 mg/kg, which persisted until 24 hours posttreatment, and had returned to control values by 48 hours. The tumor vascular volume fraction was not significantly altered over the same time course. Although the time course of response was different for diffusion MRI, tumor ADCw was also shown to be an early marker of tumor response. No change in tumor ADCw could be observed at very early time points, but a significant increase was shown 24 and 36 hours after treatment, having returned to control values by 48 hours posttreatment.

Tumor vessel permeability to MMCM has been used in the preclinical setting to assess the efficacy of different antiangiogenic therapies [27,30,32,34,50]. MMCM-enhanced MRI has been demonstrated to be capable of monitoring the direct antivascular effects of anti-VEGF antibody treatment in xenografts [51−53]. Changes in tumor vascular parameters have been measured by DCE-MRI using clinically approved small molecule contrast agents in
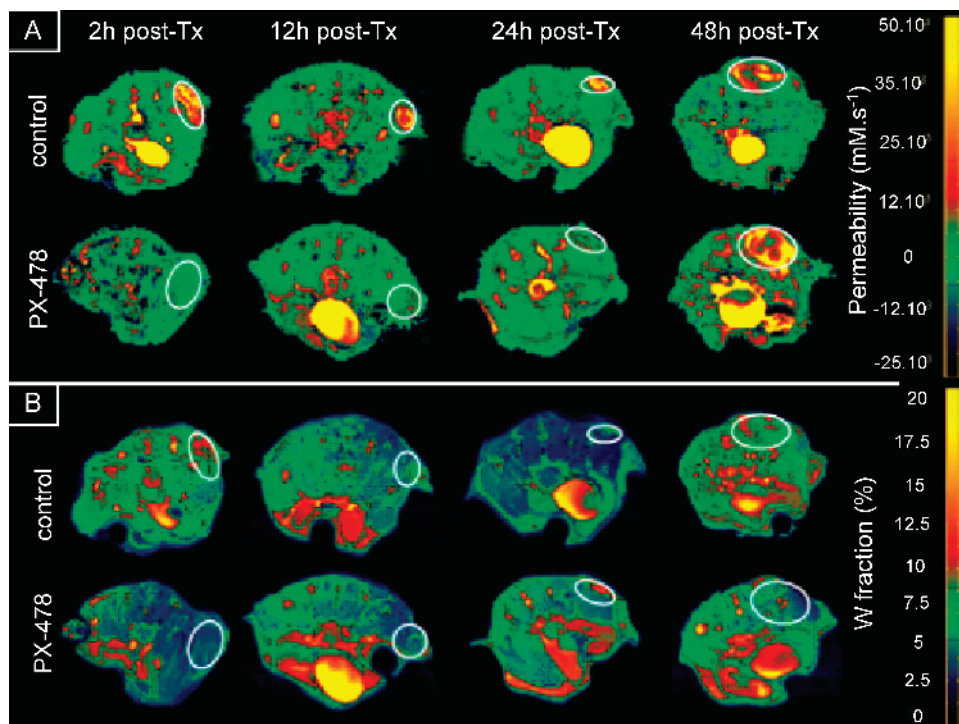
Figure 3. *(A) Permeability maps of tumors 2, 12, 24, and 48 hours after either vehicle (control) or drug (PX-478) injection. Each image represents an axial slice of the mouse with the tumor area encircled. A substantial reduction in tumor vascular permeability is observed as soon as 2 hours after PX-478 injection and until 24 hours, in comparison with the control situation. This is no longer observed by 48 hours after treatment. (B) Vascular volume fraction (VV) maps of tumors 2, 12, 24, and 48 hours after either vehicle (control) or drug (PX-478) injection. Each image represents an axial slice of the mouse with the tumor area encircled. Some individual positive or negative changes can be observed, but these were not significant between groups.*
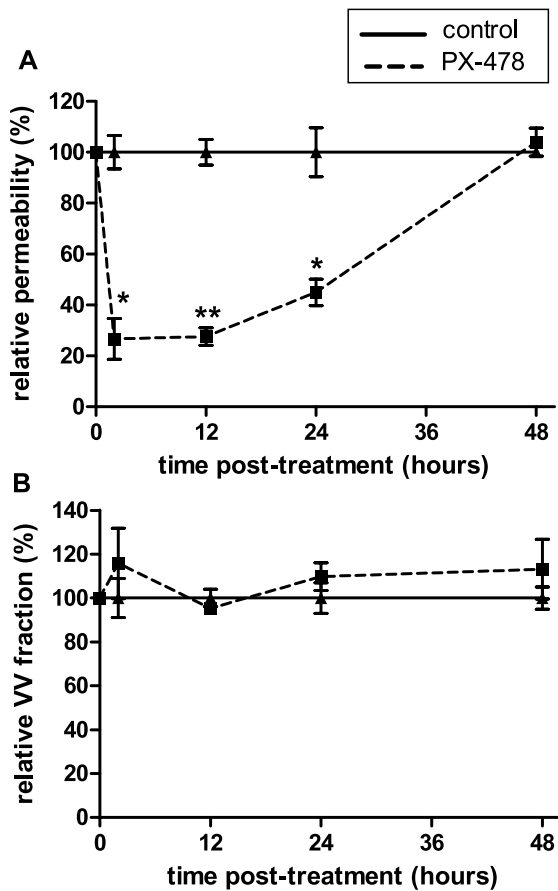
Figure 4. *Full time course of average vascular permeability (A) and vascular volume fraction (B) following administration of PX-478 (control mice, full line; treated mice, dotted line). Blood vessel permeability was estimated from the slope of the enhancement curves, and tumor vascular volume (VV) fraction was estimated from the ordinate. A significant reduction in permeability is observed 2, 12, and 24 hours after treatment with PX-478, whereas no changes are observed in the VV fraction.*

animal human tumor xenograft models following treatment with the small molecule VEGF receptor tyrosine kinase inhibitors ZD6474 [54] and PTK787/ZK222584 [55,56], and anti-VEGF antibody [57–59]. DCE-MRI studies in patients with colon cancer receiving PTK 787/ZK222584 as part of Phase I trials, while showing heterogeneity in tumor vascular response, have shown a significant correlation between tumor perfusion and the dose of PTK 787/ZK222584, with

patients with stable disease having a significantly greater reduction in the transfer constant, K^{trans}, which is related to flow, permeability, and vascular surface area [55]. Patients receiving anti-VEGF antibody as part of Phase I trial have also exhibited a reduction in tumor K^{trans} measured by DCE-MRI after the first treatment [60]. In the present study, we observed acute changes within an hour following anti-VEGF antibody therapy using the large molecular contrast agent, Gd-BSA. This suggests that the reductions in vascular permeability parameters measured by DCE-MRI were related to changes in tumor VEGF levels. In this context, PX-478 has been shown to decrease both HIF-1α and VEGF staining in HT-29 tumors [24]. However, the time course for the decrease in HIF-1α and VEGF was different from the changes in PSP measured by DCE-MRI. In our previous study, both HIF-1α and VEGF decreased within 2 hours and returned to control values by 8 hours after treatment. In contrast, in the current study, the vascular permeability estimated from MMCM kinetics was still reduced 24 hours after treatment. Also, Avastin led to changes in both vascular volume and PSP, whereas PX-478 affected only PSP, which is interpreted to be due to permeability changes alone. The differences between these responses are unknown, but may also indicate that the effect of PX-478 on hemodynamics is not mediated through VEGF. However, it also remains possible that the hemodynamics is affected by *local* concentrations or threshold values of VEGF, and these cannot yet be measured. In patients, increased VEGF expression has been correlated with the progression of colon carcinoma [61] and with the development of colon cancer metastasis [62]. In node-negative primary colon cancer, elevated tumor VEGF has been correlated with decreased patient survival [63]. Also, increased tumor VEGF expression has been associated with increased tumor angiogenesis and metastasis of human gastric cancer [64]. However, the estimation of VEGF levels is now more controversial as an accurate marker of therapeutic efficacy. Clinical studies focused on the relation between angiogenic markers (microvascular density or VEGF levels), and quantitative DCE-MRI enhancement data have shown mixed results [33,34]. Su et al. [33] concluded that the lack of correlation could be partly due to the inability of DCE-MRI with low-molecular-weight agents to reveal the true vascular function within the tumor. Bhujwalla et al. [34] recently described the

Table 1. Absolute Values of DCE-MRI Enhancement Parameters after Treatment with PX-478 or Avastin.

Tumor Model	Tx	1 hr Post-Tx		2 hr Post-Tx		12 hr Post-Tx		24 hr Post-Tx		48 hr Post-Tx	
		nP ($\times 10^{-4}$)	VV$_f$ (%)	nP ($\times 10^{-4}$)	VV$_f$ (%)	nP ($\times 10^{-4}$)	VV$_f$ (%)	nP ($\times 10^{-4}$)	VV$_f$ (%)	nP ($\times 10^{-4}$)	VV$_f$ (%)
HT-29	Control	0.65 ± 0.04	6.4 ± 0.7	0.62 ± 0.07	6.5 ± 1.2	0.62 ± 0.06	6.0 ± 0.5	0.62 ± 0.01	6.0 ± 0.8	0.60 ± 0.01	5.8 ± 0.9
	PX-478	n.d.		0.17 ± 0.09*	7.5 ± 1.8	0.17 ± 0.04**	5.7 ± 0.3	0.28 ± 0.06*	6.6 ± 0.8	0.62 ± 0.05	6.6 ± 0.7
	Avastin	0.16 ± 0.03**	4.4 ± 0.2*	n.d.							
A-549	Control	n.d.		0.35 ± 0.01	6.3 ± 0.4	n.d.					
	PX-478			0.34 ± 0.01	6.0 ± 0.7						

Normalized permeability (nP) and vascular volume fraction (VV$_f$) values (mean ± SEM) for control (carrier injection), PX-478 (125 mg/kg, i.p.), and Avastin (20 l/30 g, i.v.) groups. Note that the permeability is significantly decreased 2, 12, and 24 hours after treatment with PX-478 and within 1 hour after treatment with the anti-VEGF antibody Avastin, and that the VV$_f$ is only affected by Avastin.
*P < .05 relative to the control group (*t*-tests).
**P < .01 relative to the control group (*t*-tests).
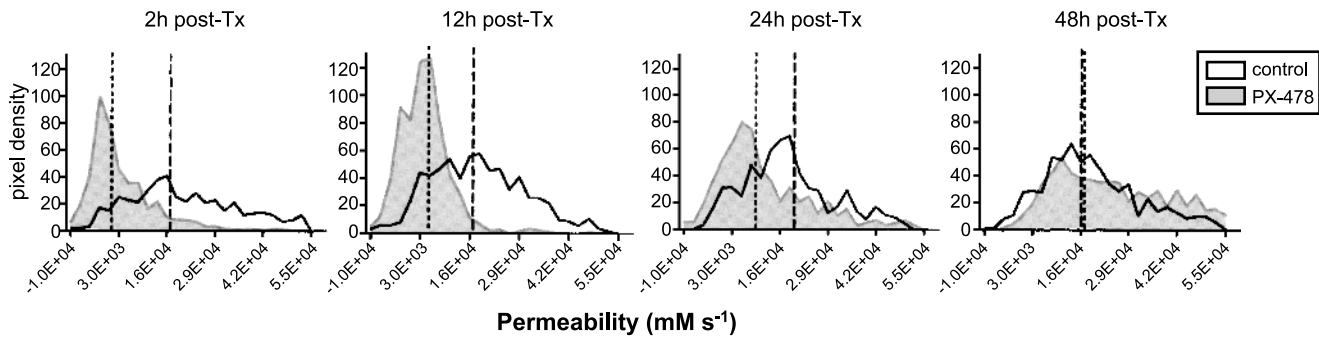
Figure 5. *Summed permeability histograms of control (open, n = 4) and treated tumors (plain, n = 4) at each time point. Note that the median (dotted line) of the treated tumors is lower than the median value of the controls. It is progressively shifted to the median of the controls over time, and is back at control values 48 hours posttreatment.*

antiangiogenic effect of the fumagillin derivative, TNP-470, by MMCM DCE-MRI. They observed a heterogeneous response, with some regions of decreased PSP and some regions with increased PSP values resulting in an apparent lack of overall response, based on the average value of tumor PSP, whereas ELISA assays detected an increase of tumor VEGF. DCE-MRI was shown to be a more reliable marker by taking into account tumor heterogeneity. Our results suggest that DCE-MRI might be a more sensitive measure of functional tumor permeability, or that permeability factors other than VEGF might be involved in the response to PX-478.

Importantly, a lack of change in the PSP of A-549 tumors between control and treated tumors was observed in this study. This correlates well with the inability of PX-478 to induce growth delays in A-549 tumors. In this case, the lack of an effect may be due to the lower baseline PSP values in A-549 compared to HT-29 tumors. It also implies that the effect of this drug on vascular parameters is mediated through the tumor cells themselves and not the host vasculature, which was the same in both tumor settings.

It has been suggested in the past that DCE-MRI could be used to monitor clinical response to anti-VEGF and inhibition of angiogenesis [54–57,65]. The current findings suggest that DCE-MRI may also be useful to assess the response to inhibition of HIF-1. However, it should be acknowledged that the current study used MMCM, which are currently unavailable in a clinical setting. These results emphasize the need to develop MMCM for monitoring antivascular therapies. Our finding that a tumor with low HIF-1α staining, which was not responsive to anti−HIF-1 therapy, also had a very low vascular PSP as measured by MMCM DCE-MRI suggests that DCE-MRI may also be useful clinically for screening and preselecting patients for therapy with anti−HIF-1 and other antiangiogenic therapies.

DW-MRI is able to detect early changes in the morphology and physiology of tissues after antineoplastic therapies. An increase in tumor ADCw could result from changes in cell membrane permeability, cell shrinkage, or vasogenic edema. Vasogenic edema results from high vessel permeability that results in the movement of osmotically active proteins and associated water to the interstitium. This mechanism is

unlikely to be the cause of increased ADC in the current system because vessel permeability decreased in response to PX-478. Both of these are associated with cell death and result in the modification of the intracellular to extracellular water populations ratio [43]. Parameters such as cell density and necrotic fraction have indeed been monitored with diffusion MRI [49,66]. In this study, we observed an increase in tumor ADCw that is consistent with other studies using other tumors and drugs [37–41,44,46,67]. In these studies,
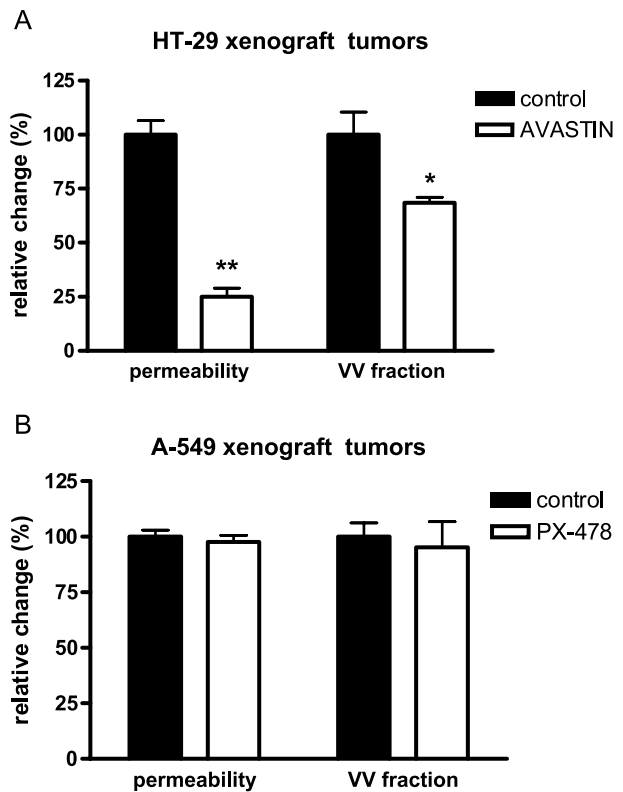
Figure 6. *(A) Relative change in HT-29 tumor vascular permeability and vascular volume fraction 1 hour after treatment with anti-VEGF antibody (Avastin). A significant reduction in permeability as well as in VV fraction is observed with this positive control. (B) Relative change in A-549 tumor (resistant to the antitumor activity of PX-478, negative control) vascular permeability, and vascular volume fraction 2 hours after treatment with PX-478. No significant change is observed in DCE parameters.*
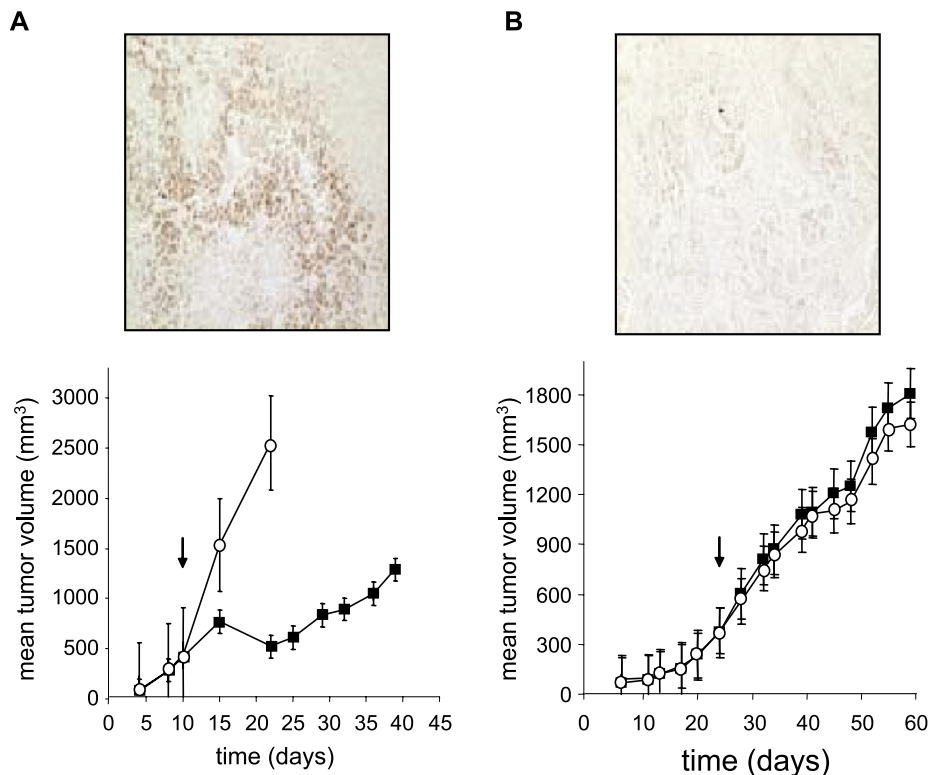
Figure 7. *HIF-1α levels and antitumor activity of PX-478 in HT-29 human colon cancer and A-549 non small cell lung cancer xenografts in SCID mice. Male SCID mice were injected subcutaneously with (A) 10^7 HT-29 human colon cancer cells or (B) A-549 non small cell lung cancer cells. The HT-29 tumors were allowed to grow to 400 mm^3 and the A-549 tumors to 360 mm^3, and treatment was begun with (○) vehicle alone or (■) PX-478 at 80 mg/kg, i.p., daily for 5 days for HT-29 xenografts and 100 mg/kg, i.p., daily for 5 days for A-549 xenografts. Treatment times are shown by arrows. The upper panels show typical immunohistochemical staining for HIF-1α in the untreated tumor xenografts at the start of the study. The lower panels show tumor xenograft growth curves. There were eight mice in each group and bars are SE.*

an increase in ADCw is correlated with ultimate tumor response, whether by apoptosis or other means of cell death. Notably, the current data document the earliest significant increase in chemotherapy-induced ADCw. Previous reports have indicated that the earliest significance was not reached until 48 hours following therapy [36,39].

The combination of dynamic and DW MRI in the follow-up of chemotherapy has been used in the past [68,69] and has been proven to be of good predictive value for therapy outcome in patients with primary rectal carcinoma [70]. In this study, the acquisition of both DW and DCE images in a single protocol on the same animal allowed us to coregister these data and compare the two techniques. We define the *dynamic range* (DR) as the maximum change relative to the variance of controls. For these studies, the DR was higher for DW-MRI (maximum effect at 24 hours, DR = 8.7) than for DCE-MRI (maximum effect at 2 hours, DR = 3.2). Tumor ADCw was thereby shown to be a sensitive and early marker of tumor response in this study. Nonetheless, the DCE-MRI response preceded the diffusion response and opened up the possibility of monitoring acute effects of drug *in vivo*. The combination of the two techniques gives unique insights into the complex response of HT-29 tumors to PX-478 by showing very early changes in vascular permeability followed by large changes in cellularity. Considering the magnitude of response of HT-29 xenografts to PX-478 observed

with early and sensitive markers, we can speculate that noninvasive monitoring of PX-478 by DCE and/or diffusion MRI will be of particular interest in the clinic.

References

[1] Hoeckel M, Schlenger K, Aral B, Mitza M, Schaffer U, and Vaupel P (1996). Association between tumour hypoxia and malignant progression in advanced cancer of the uterine cervix. *Cancer Res* **56**, 4509–4515.

[2] Moulder J and Rockwell S (1987). Tumor hypoxia: its impact on cancer therapy. *Cancer Metastasis Rev* **5**, 313–341.

[3] Nordsmark M, Hoyer M, Keller J, Nielson OS, Jensen OM, and Overgaard J (1996). The relationship between tumor oxygenation

and cell proliferation in human soft tissue sarcomas. *Int J Radiat Oncol Biol Phys* **35**, 701–708.

[4] Goonewardene TI, Sowter HM, and Harris AL (2002). Hypoxia-induced pathways in breast cancer. *Micro Res Tech* **59**, 41–48.

[5] Chen J, Zhao S, Nakada K, Kuge Y, Tamaki N, Okada F, Wang J, Shindo M, Higashino F, Takeda K, Asaka M, Katoh H, Sugiyama T, Hosokawa M, and Kobayashi M (2003). Dominant-negative hypoxia-inducible factor-1α reduces tumorigenicity of pancreatic cancer cells through the suppression of glucose metabolism. *Am J Pathol* **162**, 1283–1291.

[6] Hanahan D and Folkman J (1996). Patterns and emerging mechanisms of the angiogenic switch during tumorigenesis. *Cell* **86**, 353–364.

[7] Semenza GL (2000). HIF-1: mediator of physiological and pathophysiological responses to hypoxia. *J Am Phys Soc* **88**, 1474–1480.

[8] Powis G and Kirkpatrick L (2004). HIF-1α as a cancer drug target. *Mol Cancer Ther* **3**, 647–654.

[9] Wang G, Dong Z, Xu G, Yang Z, Shou C, Wang N, and Liu T (1998). The effect of antibody against vascular endothelial growth factor on tumor growth and metastasis. *J Cancer Res Clin Oncol* **124**, 615–620.

[10] Chilov D, Camneish G, Kvietikova I, Ziegler U, Gassmann M, and Wenger RH (1999). Induction and nuclear translocation of hypoxia-inducible factor-1 (HIF-1): heterodimerization with ARNT is not necessary for nuclear accumulation of HIF-1α. *J Cell Sci* **112**, 1203–1212.

[11] Minchenko A, Salceda S, and Bauer T (1994). Hypoxia regulatory elements of the human vascular endothelial growth factor gene. *Cell Mol Biol Res* **40**, 35–39.

[12] Kallio PJ, Wilson WJ, O'Brien S, Makino Y, and Poellinger L (1999). Regulation of the hypoxia-inducible factor-1α by the ubiquitin–proteosome pathway. *J Biol Chem* **274**, 6519–6525.

[13] Huang TT, Yasunami M, Carlson EJ, Gillespie AM, Reaume AG, Hoffman EK, Chan PH, Scott RW, and Epstein CJ (1997). Superoxide-mediated cytotoxicity in superoxide dismutase–deficient fetal fibroblasts. *Arch Biochem Biophys* **344**, 424–432.

[14] Zhong H, De Marzo AM, Laughner E, Lim M, Hilton DA, Zagzag D, Buechler P, Isaacs WB, Semenza GL, and Simons JW (1999). Overexpression of hypoxia-inducible factor 1 alpha in common human cancers and metastases. *Cancer Res* **59**, 5830–5835.

[15] Giatromanolaki A, Koukourakis M, Sivridis E, Turley H, and Talks K (2001). Relation of hypoxia inducible factor 1 alpha and 2 alpha in operable non-small cell lung cancer to angiogenic molecular profile of tumors and survival. *Br J Cancer* **85**, 881–890.

[16] Birner P, Schindl M, Obermair A, Breitenecker G, and Oberhuber G (2001). Expression of hypoxia-inducible factor-1 alpha in epithelial ovarian tumors: its impact on prognosis and on response to chemotherapy. *Clin Cancer Res* **7**, 1661–1668.

[17] Bos R, van der Groep P, Greijer AE, Shvarts A, Meijer S, Pinedo HM, Semenza GL, van Diest PJ, and van der Wall E (2003). Levels of hypoxia-inducible factor-1alpha independently predict prognosis in patients with lymph node negative breast carcinoma. *Cancer* **97**, 1573–1581.

[18] Aebersold DM, Burri P, Beer KT, Laissue J, Djonov V, Greiner RH, and Semenza GL (2001). Expression of hypoxia-inducible factor-1alpha: a novel predictive and prognostic parameter in the radiotherapy of oropharyngeal cancer. *Cancer Res* **61**, 2911–2916.

[19] Birner P, Schindl M, Obermair A, Plank C, Breitenecker G, and Oberhuber G (2000). Over-expression of hypoxia-inducible factor-1alpha is a marker for an unfavorable prognosis in early-stage invasive cervical cancer. *Cancer Res* **60**, 4693–4696.

[20] Semenza GL (2000). Hypoxia, clonal selection, and the role of HIF-1 in tumor progression. *Crit Rev Biochem Mol Biol* **35**, 71–103.

[21] Zagzag D, Zhong H, Scalzetti J, Laughner E, Simons J, Semenza G (2000). Expression of hypoxia-inducible factor-1 alpha in brain tumors: association with angiogenesis, invasion and progression. *Cancer* **88**, 2606–2618.

[22] Pietsch T, Valter MM, Wolf HK, von Deimling A, Huang HJ, Cavenee WK, and Wiestler OD (1997). Expression and distribution of vascular endothelial growth factor protein in human brain tumors. *Acta Neuropathol* **93**, 109–117.

[23] Takano S, Yoshii Y, Kondo S, Suzuki H, Maruno T, Shirai S, and Nose T (1996). Concentration of vascular endothelial growth factor in the serum and tumor tissue of brain tumor patients. *Cancer Res* **56**, 2185–2190.

[24] Welsh S, Williams R, Kirkpatrick L, Paine-Murrieta G, and Powis G (2004). Antitumor activity and pharmacodynamic properties of PX-478, an inhibitor of hypoxia-inducible factor-1alpha. *Mol Cancer Ther* **3** (3), 233–244.

[25] Gillies RJ, Bhujwalla ZM, Evelhoch J, Garwood M, Neeman M, Robinson SP, Sotak CH, and Van Der Sanden B (2000). Applications of magnetic resonance in model systems: tumor biology and physiology. *Neoplasia* **2** (1–2), 139–151.

[26] Evelhoch JL, Gillies RJ, Karczmar GS, Koutcher JA, Maxwell RJ, Nalcioglu O, Raghunand N, Ronen SM, Ross BD, and Swartz HM (2000). Applications of magnetic resonance in model systems: cancer therapeutics. *Neoplasia* **2** (1–2), 152–165.

[27] Padhani AR (2002). Dynamic contrast-enhanced MRI in clinical oncology: current status and future directions. *J Magn Reson Imaging* **16** (4), 407–422.

[28] Knopp MV, Giesel FL, Marcos H, von Tengg-Kobligk H, and Choyke P (2001). Dynamic contrast-enhanced magnetic resonance imaging in oncology. *Top Magn Reson Imaging* **12** (4), 301–308.

[29] Brasch R, Pham C, Shames D, Roberts T, van Dijke K, van Bruggen N, Mann J, Ostrowitzki S, and Melnyk O (1997). Assessing tumor angiogenesis using macromolecular MR imaging contrast media. *J Magn Reson Imaging* **7** (1), 68–74.

[30] Demsar F, Roberts TP, Schwickert HC, Shames DM, van Dijke CF, Mann JS, Saeed M, and Brasch RC (1997). A MRI spatial mapping technique for microvascular permeability and tissue blood volume based on macromolecular contrast agent distribution. *Magn Reson Med* **37** (2), 236–242.

[31] Gossmann A, Okuhata Y, Shames DM, Helbich TH, Roberts TP, Wendland MF, Huber S, and Brasch RC (1999). Prostate cancer tumor grade differentiation with dynamic contrast-enhanced MR imaging in the rat: comparison of macromolecular and small-molecular contrast media—preliminary experience. *Radiology* **213** (1), 265–272.

[32] Daldrup H, Shames DM, Wendland M, Okuhata Y, Link TM, Rosenau W, Lu Y, and Brasch RC (1998). Correlation of dynamic contrast-enhanced MR imaging with histologic tumor grade: comparison of macromolecular and small-molecular contrast media. *AJR Am J Roentgenol* **171** (4), 941–949.

[33] Su MY, Cheung YC, Fruehauf JP, Yu H, Nalcioglu O, Mechetner E, Kyshtoobayeva A, Chen SC, Hsueh S, McLaren CE, and Wan YL (2003). Correlation of dynamic contrast enhancement MRI parameters with microvessel density and VEGF for assessment of angiogenesis in breast cancer. *J Magn Reson Imaging* **18** (4), 467–477.

[34] Bhujwalla ZM, Artemov D, Natarajan K, Solaiyappan M, Kollars P, and Kristjansen PE (2003). Reduction of vascular and permeable regions in solid tumors detected by macromolecular contrast magnetic resonance imaging after treatment with antiangiogenic agent TNP-470. *Clin Cancer Res* **9** (1), 355–362.

[35] Bammer R (2003). Basic principles of diffusion-weighted imaging. *Eur J Radiol* **45** (3), 169–184.

[36] Zhao M, Pipe JG, Bonnett J, and Evelhoch JL (1996). Early detection of treatment response by diffusion-weighted ^{1}H-NMR spectroscopy in a murine tumour *in vivo*. *Br J Cancer* **73** (1), 61–64.

[37] Hakumaki JM, Poptani H, Puumalainen AM, Loimas S, Paljarvi LA, Yla-Herttuala S, and Kauppinen RA (1998). Quantitative ^{1}H nuclear magnetic resonance diffusion spectroscopy of BT4C rat glioma during thymidine kinase–mediated gene therapy *in vivo*: identification of apoptotic response. *Cancer Res* **58** (17), 3791–3799.

[38] Poptani H, Puumalainen AM, Grohn OH, Loimas S, Kainulainen R, Yla-Herttuala S, and Kauppinen RA (1998). Monitoring thymidine kinase and ganciclovir-induced changes in rat malignant glioma *in vivo* by nuclear magnetic resonance imaging. *Cancer Gene Ther* **5** (2), 101–109.

[39] Chenevert TL, Stegman LD, Taylor JM, Robertson PL, Greenberg HS, Rehemtulla A, and Ross BD (2000). Diffusion magnetic resonance imaging: an early surrogate marker of therapeutic efficacy in brain tumors. *J Natl Cancer Inst* **92** (24), 2029–2036.

[40] Mardor Y, Roth Y, Lidar Z, Jonas T, Pfeffer R, Maier SE, Faibel M, Nass D, Hadani M, Orenstein A, Cohen JS, and Ram Z (2001). Monitoring response to convection-enhanced taxol delivery in brain tumor patients using diffusion-weighted magnetic resonance imaging. *Cancer Res* **61** (13), 4971–4973.

[41] Mardor Y, Roth Y, Ochershvilli A, Spiegelmann R, Tichler T, Daniels D, Maier SE, Nissim O, Ram Z, Baram J, Orenstein A, and Pfeffer R (2004). Pretreatment prediction of brain tumors response to radiation therapy using high *b*-value diffusion-weighted MRI. *Neoplasia* **6** (2), 136–142.

[42] Norris DG (2001). The effects of microscopic tissue parameters on the diffusion weighted magnetic resonance imaging experiment. *NMR Biomed* **14** (2), 77–93.

[43] Kauppinen RA (2002). Monitoring cytotoxic tumour treatment response by diffusion magnetic resonance imaging and proton spectroscopy. *NMR Biomed* **15** (1), 6–17.

[44] Ross BD, Moffat BA, Lawrence TS, Mukherji SK, Gebarski SS, Quint DJ, Johnson TD, Junck L, Robertson PL, Muraszko KM, Dong Q, Meyer CR, Bland PH, McConville P, Geng H, Rehemtulla A, and Chenevert TL (2003). Evaluation of cancer therapy using diffusion magnetic resonance imaging. *Mol Cancer Ther* **2** (6), 581–587.

[45] Galons JP, Altbach MI, Paine-Murrieta GD, Taylor CW, and Gillies RJ (1999). Early increases in breast tumor xenograft water mobility in response to paclitaxel therapy detected by non-invasive diffusion magnetic resonance imaging. *Neoplasia* **1** (2), 113–117.

[46] Jennings D, Hatton BN, Guo J, Galons JP, Trouard TP, Raghunand N, Marshall J, and Gillies RJ (2002). Early response of prostate carcinoma xenografts to docetaxel chemotherapy monitored with diffusion MRI. *Neoplasia* **4** (3), 255–262.

[47] Theilmann RJ, Borders R, Trouard TP, Xia G, Outwater E, Ranger-Moore J, Gillies RJ, and Stopeck A (2005). Changes in water mobility measured by diffusion MRI predict response of metastatic breast cancer to chemotherapy. *Neoplasia* (in press).

[48] Trouard TP, Theilmann RJ, Altbach MI, and Gmitro AF (1999). High-resolution diffusion imaging with DIFRAD-FSE (diffusion-weighted radial acquisition of data with fast spin-echo) MRI. *Magn Reson Med* **42** (1), 11–18.

[49] Lyng H, Haraldseth O, and Rofstad EK (2000). Measurement of cell density and necrotic fraction in human melanoma xenografts by diffusion weighted magnetic resonance imaging. *Magn Reson Med* **43** (6), 828–836.

[50] Marzola P, Degrassi A, Calderan L, Farace P, Crescimanno C, Nicolato E, Giusti A, Pesenti E, Terron A, Sbarbati A, Abrams T, Murray L, and Osculati F (2004). *In vivo* assessment of antiangiogenic activity of SU6668 in an experimental colon carcinoma model. *Clin Cancer Res* **10,** 739–750.

[51] Pham CD, Roberts TP, van Bruggen N, Melnyk O, Mann J, Ferrara N, Cohen RL, and Brasch RC (1998). Magnetic resonance imaging detects suppression of tumor vascular permeability after administration of antibody to vascular endothelial growth factor. *Cancer Invest* **16** (4), 225–230.

[52] Roberts TP, Turetschek K, Preda A, Novikov V, Moeglich M, Shames DM, Brasch RC, and Weinmann HJ (2002). Tumor microvascular changes to anti-angiogenic treatment assessed by MR contrast media of different molecular weights. *Acad Radiol* **9,** S511–S513.

[53] Turetschek K, Preda A, Floyd E, Shames DM, Novikov V, Roberts TP, Wood JM, Fu Y, Carter WO, and Brasch RC (2002). MRI monitoring of tumor response to a novel VEGF tyrosine kinase inhibitor in an experimental breast cancer model. *Acad Radiol* **2,** S519–S520.

[54] Checkley D, Tessier JJ, Kendrew J, Waterton JC, and Wedge SR (2003). Use of dynamic contrast-enhanced MRI to evaluate acute treatment with ZD6474, a VEGF signalling inhibitor, in PC-3 prostate tumours. *Br J Cancer* **89** (10), 1889–1895.

[55] Morgan B, Thomas AL, Drevs J, Hennig J, Buchert M, Jivan A, Horsfield MA, Mross K, Ball HA, Lee L, Mietlowski W, Fuxius S, Unger C, O'Bryne K, Henry A, Cherryman GR, Laurent D, Dugan M, Marme D, and Steward WP (2003). Dynamic contrast-enhanced magnetic resonance imaging as a biomarker for the pharmacological response of PTK787/ZK 222584, an inhibitor of the vascular endothelial growth factor receptor tyrosine kinases, in patients with advanced colorectal cancer and liver metastases: results from two phase I studies. *J Clin Oncol* **21** (21), 3955–3964.

[56] Turetschek K, Preda A, Floyd E, Shames DM, Novikov V, Roberts TP, Wood JM, Fu Y, Carter WO, and Brasch RC (2003). MRI monitoring of tumor response following angiogenesis inhibition in an experimental human breast cancer model. *Eur J Nucl Med Mol Imaging* **30** (3), 448–455.

[57] Gossmann A, Helbich TH, Kuriyama N, Ostrowitzki S, Roberts TP, Brasch RC, van Bruggen N, Wendland MF, Israel MA, and Brasch RC (2002). Dynamic contrast-enhanced magnetic resonance imaging as a surrogate marker of tumor response to anti-angiogenic therapy in a xenograft model of glioblastoma multiforme. *J Magn Reson Imaging* **15** (3), 233–240.

[58] Kiessling F, Farhan N, Lichy MP, Vosseler S, Heilmann M, Krix M, Bohlen P, Miller DW, Mueller MM, Semmler W, Fusenig NE, and Delorme S (2004). Dynamic contrast-enhanced magnetic resonance imaging rapidly indicates vessel regression in human squamous cell carcinomas grown in nude mice caused by VEGF receptor 2 blockade with DC101. *Neoplasia* **6** (3), 213–223.

[59] Turetschek K, Preda A, Novikov V, Brasch RC, Weinmann HJ, Wunderbaldinger P, and Roberts TP (2004). Tumor microvascular changes in antiangiogenic treatment: assessment by magnetic resonance contrast media of different molecular weights. *J Magn Reson Imaging* **20** (1), 138–144.

[60] Jayson GC, Zweit J, Jackson A, Mulatero C, Julyan P, Ranson M, Broughton L, Wagstaff J, Hakannson L, Groenewegen G, Bailey J, Smith N, Hastings D, Lawrance J, Haroon H, Ward T, McGown AT, Tang M, Levitt D, Marreaud S, Lehmann FF, Herold M, and Zwierzina H (2002). Molecular imaging and biological evaluation of HuMV833 anti-VEGF antibody: implications for trial design of antiangiogenic antibodies. *J Natl Cancer Inst* **94** (19), 1484–1493.

[61] Wong MP, Cheung N, Yuen ST, Leung SY, and Chung LP (1999). Vascular endothelial growth factor is upregulated in early premalignant stage of colorectal tumour progression. *Int J Cancer* **81,** 845–850.

[62] Okamoto K, Oshika Y, Fukushima Y, Yoshimura M, Ohnishi Y, Tokunaga T, Hashimoto T, Hatanaka H, Tomii Y, Yoshida Y, Miura S, Tsuchida T, Kijima H, Yamazaki H, Nakamura M, and Ueyama Y (1999). Inhibition of liver metastasis of colon cancer by in vivo administration of anti-vascular endothelial growth factor antibody. *Oncol Rep* **6** (3), 553–556.

[63] Wang GL, Jiang BH, and Rue EA (1995). Hypoxia-inducible factor I is a basic–helix–loop–helix–PAS heterodimer regulated by cellular O$_2$ tension. *Proc Natl Acad Sci USA* **92,** 5510–5514.

[64] Yonemura Y, Endo Y, Fujita H, Fishida S, Ninomiya I, Bandou E, Taniguchi K, Miwa K, Ohoyama S, Sugiyama K, and Sasaki T (1999). Role of vascular endothelial growth factor C expression in the development of lymph node metastasis in gastric cancer. *Clin Cancer Res* **5,** 1823–1829.

[65] Thomas AL, Morgan B, Drevs J, Unger C, Wiedenmann B, Vanhoefer U, Laurent D, Dugan M, and Steward WP (2003). Vascular endothelial growth factor receptor tyrosine kinase inhibitors: PTK787/ZK 222584. *Semin Oncol* **30** (3), 32–38.

[66] Helmer KG, Meiler MR, Sotak CH, and Petruccelli JD (2003). Comparison of the return-to-the-origin probability and the apparent diffusion coefficient of water as indicators of necrosis in RIF-1 tumors. *Magn Reson Med* **49** (3), 468–478.

[67] Stegman LD, Rehemtulla A, Hamstra DA, Rice DJ, Jonas SJ, Stout KL, Chenevert TL, and Ross BD (2000). Diffusion MRI detects early events in the response of a glioma model to the yeast cytosine deaminase gene therapy strategy. *Gene Ther* **7** (12), 1005–1010.

[68] Beauregard DA, Pedley RB, Hill SA, and Brindle KM (2002). Differential sensitivity of two adenocarcinoma xenografts to the anti-vascular drugs combretastatin A4 phosphate and 5,6-dimethylxanthenone-4-acetic acid, assessed using MRI and MRS. *NMR Biomed* **15** (2), 99–105.

[69] Sinha S and Sinha U (2002). Functional magnetic resonance of human breast tumors: diffusion and perfusion imaging. *Ann N Y Acad Sci* **980,** 95–115.

[70] DeVries AF, Kremser C, Hein PA, Griebel J, Krezcy A, Ofner D, Pfeiffer KP, Lukas P, and Judmaier W (2003). Tumor microcirculation and diffusion predict therapy outcome for primary rectal carcinoma. *Int J Radiat Oncol Biol Phys* **15; 56** (4), 958–965.